Measuring intensity correlations with a two-element superconducting nanowire single-photon detector

Eric A. Dauler,[1,2] Martin J. Stevens,[3] Burm Baek,[3] Richard J. Molnar,[2] Scott A. Hamilton,[2] Richard P. Mirin,[3] Sae Woo Nam,[3] and Karl K. Berggren[1]

[1]*Research Laboratory of Electronics, Massachusetts Institute of Technology, Cambridge, Massachusetts 02139, USA*

[2]*Lincoln Laboratory, Massachusetts Institute of Technology, Lexington, Massachusetts 02420, USA*

[3]*National Institute of Standards and Technology, 325 Broadway, Boulder, Colorado 80305, USA*

(Received 12 May 2008; published 24 November 2008)

Second-order intensity correlation measurements were made using a two-element superconducting nanowire single photon detector (SNSPD) without the need for an optical beam splitter. This approach can be used to obtain a 50-ps full width at half maximum timing resolution over a wide range of visible and near-infrared wavelengths and can be extended to measure higher-order intensity correlations. Measurements of the second-order intensity correlation of a pulsed laser and an InGaAs quantum dot were made using both a two-element SNSPD and a conventional Hanbury Brown–Twiss interferometer to demonstrate the accuracy and advantages of the multielement SNSPD.

DOI: 10.1103/PhysRevA.78.053826 PACS number(s): 42.50.Ar, 85.25.Oj, 42.50.Dv, 03.67.Dd

I. INTRODUCTION

Intensity correlation measurements are one of the key techniques for characterizing photon statistics and identifying effects such as bunching [1] and antibunching [2], which can reveal important information about the physics governing emission. Instead of directly measuring the photon statistics, which are affected by loss and detector imperfections, intensity correlations can be measured using a Hanbury Brown–Twiss (HBT) interferometer geometry, which consists of a beam splitter and two discrete single-photon detectors [1]. The beam splitter serves to split the light into each of its output modes, so that both detectors sample light from the spatial modes of interest and intensity correlations for a stationary source are a function only of time delay (τ) [3]:

$$g^{(2)}(\tau) = \frac{\langle :\hat{I}(t)\hat{I}(t+\tau): \rangle}{\langle \hat{I}(t) \rangle^2}, \tag{1}$$

where :: denotes normal ordering of the creation and annihilation operators contained in the intensity operator $\hat{I}$.

Alternatively, a single detector can be used to measure temporal intensity correlations [4], eliminating possible artifacts with the HBT interferometer including discrete detectors aligned to different spatial modes or spurious reflections off the beam splitter. However, using a single detector typically prevents or complicates correlation measurements at small time delays. The finite recovery time of the analog-output signal from a photon-number-resolving (PNR) detector makes it difficult to independently resolve and accurately time all closely spaced detection events. With a single non-PNR detector, correlation measurements are limited to time delays longer than the dead time of the detector and electronics.

In this paper, the advantages of both the two-detector HBT interferometer and the single detector approaches are achieved simultaneously by using a two-element superconducting nanowire single-photon detector (SNSPD). These advantages are demonstrated by measuring intensity correlations of a laser and a quantum dot single-photon source.

II. MULTIELEMENT DETECTOR AND EXPERIMENTAL SETUP

The desirable features of discrete SNSPDs for measuring intensity correlation functions have been previously demonstrated [5–9]. The SNSPD is composed of an ~5-nm-thick, ~100-nm-wide superconducting wire at the end of a transmission line through which current is passed. When correctly biased, the absorption of a single photon can temporarily destroy the superconductivity, shunting current into the transmission line where it is measured as a voltage pulse. The detectors provide a Gaussian-shaped instrument response function (IRF) with a $<30-100$-ps full width at half maximum (FWHM) [5–10]. The devices can be packaged for operation in a closed-cycle cryocooler [5] or helium storage dewar [8] with a single-mode optical fiber that achieves system detection efficiencies of 1%–10% over a wide range of wavelengths; incorporating a multi-element design and optical cavity can result in a system detection efficiency of >25% [11]. In contrast to Geiger-mode InGaAs avalanche photodiodes, which are typically operated in gated mode because of high dark count rates and long "hold-off" times needed to prevent afterpulsing, SNSPDs can be operated continuously (ungated) because SNSPDs have low dark-count rates and negligible afterpulsing, while self-resetting in only a few to few tens of nanoseconds [12]. This performance has enabled measurements of fast photoluminescence (PL) [8,9,13] and second-order intensity correlation functions [5–9] over a range of near-infrared wavelengths.

In this work, a multielement SNSPD [10,11] was used to make intensity correlation measurements, without the need for a beam splitter or the disadvantages of using an analog-output PNR detector. A multielement SNSPD has the same meander-wire arrangement as a single SNSPD, except that multiple, electrically isolated wires are formed by making breaks in the wire outside the active area. Consequently, tem-

poral intensity correlations can be measured between independent elements in the same way as with discrete detectors. This capability prevents extra correlations that would be introduced by a PNR detector if the detection efficiency or ability to correctly resolve detection events varied when photons were nearly simultaneous, which can be a problem for PNR detectors with low signal-to-noise ratios or for photons incident during the detector recovery. Furthermore, the output signal from each multi-element SNSPD detector can be analyzed using standard time-correlated single photon counting (TCSPC) hardware, and the photon timing can be precisely resolved independent of the time delay between photons [10,11]. Finally, as with any PNR detector, using a single active area eliminates the need for a beam splitter, simplifying the optical setup and eliminating artifacts such as discrete detectors aligned to different spatial modes or spurious reflections off the beam splitter.

Multielement SNSPDs also provide detector-performance advantages relative to a single SNSPD, allowing the multielement SNSPD approach to further outperform two discrete SNSPDs with a beam splitter. If the active area, which is set by the need to maintain efficient optical coupling, is divided into multiple independent elements, each element will have shorter rise and reset times due to its lower inductance [12]. If the elements are addressed independently, as is the case for the multielement SNSPD, the bias current for each wire can be set independently, allowing each wire to be optimally biased. Finally, integrating multiple elements in a single active area increases the probability of obtaining a high-detection-efficiency device, because this probability is limited by statistical variations in both the constriction-limited detection efficiency [14] and the fiber-coupling loss.

In order to demonstrate the validity and advantages of the multielement SNSPD, this approach was compared to a conventional HBT interferometer using the experimental setup shown in Fig. 1. The single-photon source consisted of a self-assembled InGaAs quantum dot buried in a vertical micropillar cavity [6] that was cooled to ~5 K in a liquid-helium flow cryostat. The quantum dot was excited using a mode-locked Ti:sapphire laser producing ~1-ps pulses at 82 MHz repetition frequency and 779 nm center wavelength. This light was attenuated to ~200 nW average power and focused using a long-working-distance objective to a spot size of ~5 μm so that it excited only a single micropillar. The same objective collected the PL emitted at 959.7 nm from the quantum dot, which was filtered using a monochromator and sent into either the free-space HBT with two silicon single-photon avalanche diodes (SPADs) [15] [Fig. 1(b)] or collected in a single-mode (at 1550 nm wavelength) fiber for delivery to the two-element SNSPD [Fig. 1(c)].

The two-element SNSPD was designed as a linear array of four SNSPDs, each with a 5 μm by 10 μm area such that any two adjacent SNSPDs formed a 10 μm by 10 μm active area [Fig. 1(d)]. NbN films were deposited at MIT Lincoln Laboratory [16], and the devices were fabricated, without optical cavities, at MIT using a previously described process [17] with several recent modifications [11]. The chip was packaged with an optical fiber aligned just above the detector [5], in a mount modified to include two coaxial electrical connectors, wire bonded to the two elements on which the fiber was centered. The detector package was installed and operated at a stable, ~3 K temperature in a closed-cycle cryocooler.

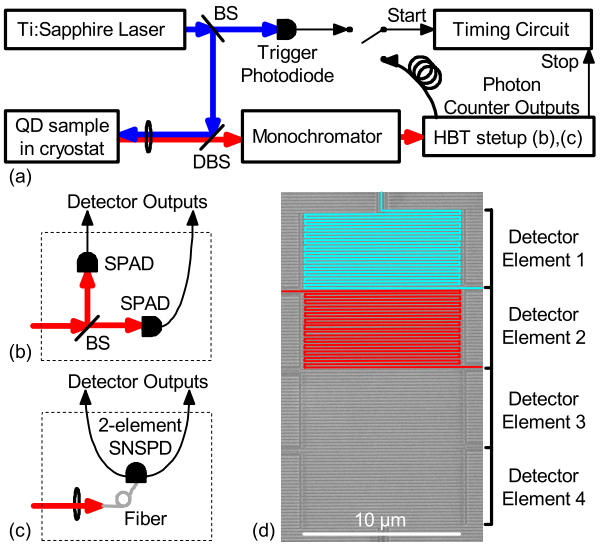

FIG. 1. (Color online) (a) Experimental schematic for the IRF and PL lifetime measurements (start input connected to the trigger photodiode) and the $g^{(2)}(0)$ measurements (start input connected to the photon counter). BS, beam splitter; DBS, dichroic beam splitter. Schematic of the Hanbury Brown–Twiss setup using (b) a free-space beam splitter and two discrete SPADs and (c) a fiber-coupled two-element SNSPD. A scanning-electron micrograph of the SNSPD is shown in (d) with two of the elements highlighted for clarity. The fiber is aligned to the best two adjacent elements.

III. MEASUREMENT RESULTS

The IRF of each of the detectors and the PL lifetime of the quantum dot were first measured. To measure the IRFs, the detectors were illuminated with Ti:sapphire laser pulses (monochromator tuned to 779 nm), and for the PL measurements, the 959.7-nm monochromator-filtered output from the quantum dot sample was used [Fig. 1(a)]. The output from an illuminated detector was then connected to the start channel of the TCSPC hardware [15], and a portion of the light from the Ti:sapphire laser was focused onto a fast photodiode connected to the stop channel.

The results for one SPAD and one SNSPD are shown in Fig. 2; nearly identical results were achieved using the other SPAD and the other SNSPD (not shown). The SNSPD has a narrower IRF than the SPAD, with no measurable tail, and consequently can resolve the PL lifetime of the quantum dot easily without deconvolution techniques. Although deconvolution may allow PL lifetimes equal to or even shorter than the detector IRF to be accurately measured and SPADs with narrower IRF FWHM than the ones used in these experiments are available, the SNSPD's narrow, Gaussian-shaped IRF is ideally suited to PL lifetime measurements [13].

Second-order temporal intensity correlations were also measured using either the two-element SNSPD or the two SPADs. The same setup (Fig. 1) was used in this case, except the start channel of the timing circuit was connected to the

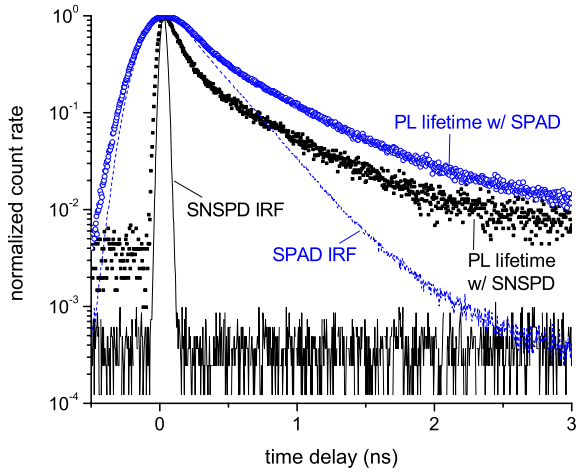

FIG. 2. (Color online) Measurements of IRFs (SNSPD, black solid line; SPAD, blue dotted line) and PL lifetimes (SNSPD, black solid squares; SPAD, blue open circles). The 50-ps-FWHM, Gaussian-shaped SNSPD IRF allows the quantum dot lifetime to be measured more accurately.

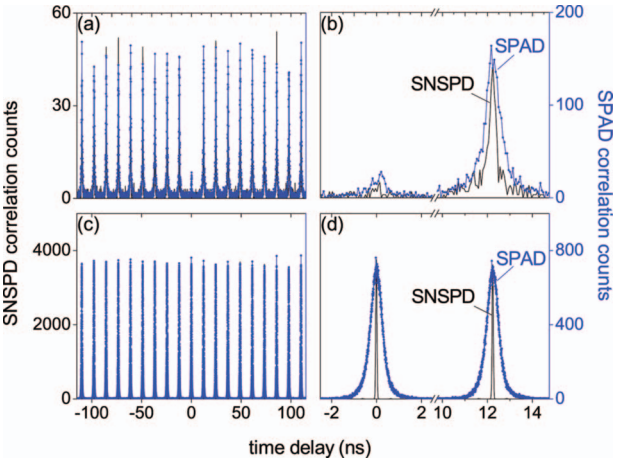

FIG. 3. (Color) Measured intensity correlation histograms for the quantum dot single-photon source (a),(b) and the Ti:sapphire laser (c),(d). The measurements were made with the two-element SNSPD (solid black lines) and, subsequently, with the SPAD-based HBT setup (blue lines with solid circles). The shape and width of the peaks demonstrate that the two-element SNSPD may be used to achieve improved timing resolution, while the setup-independent ratio of counts in the zero-time-delay peak relative to the counts in the other peaks demonstrates that both detector setups can be used to accurately measure $g^{(2)}(0)$.

output from the second SPAD or the second element of the SNSPD, rather than the trigger photodiode, and an ~100-ns-long coaxial cable was used to delay the stop, to permit measuring correlations with both positive and negative time delays. A truly single-mode fiber (at 780 and 960 nm wavelength) would have ensured that both detector elements were illuminated with the same spatial mode, but the fiber used (single mode at 1550 nm wavelength) can support more than one spatial mode at the wavelengths of interest. Instead, the lack of spatial correlations in the sources investigated here helped ensure that only temporal correlations were measured. An interleaved detector design [11] is preferable in the future to ensure that both elements sample the same spatial mode(s).

The measured intensity correlations for the quantum dot single-photon source are shown in Figs. 3(a) and 3(b) and the intensity correlations of the Ti:sapphire laser are shown in Figs. 3(c) and 3(d), with the monochromator tuned to the same wavelengths used for the PL and IRF measurements. The pulsed (non-stationary) source results in peaks in the intensity correlation histogram at time delays corresponding to the pulse repetition period. The width of the correlation peaks measured with the SNSPD are limited by the IRF for the pulsed laser [Fig. 3(b)] and by the PL lifetime for the quantum dot [Fig. 3(d)]. The narrow IRF of the SNSPD provides a high-resolution measurement of the photon correlations from the quantum dot and allows correlations with time delays less than the PL lifetime to be examined, which cannot be resolved with the SPAD due to its long IRF.

The pulsed nature of the source also requires $g^{(2)}(0)$ to be calculated differently than in a stationary source: here, $g^{(2)}(0)$ is calculated by dividing the total number of counts in the peak at zero time delay by the average number of counts in peaks at nonzero time delays. The data for nine peaks on each side of zero delay are plotted [Figs. 3(a) and 3(c)] and used to calculate $g^{(2)}(0)$, since this was a reasonable compromise between minimizing statistical variations and minimizing the systematic decrease in coincidences at later time delays (some long-delay coincidence events were blocked due to the single-stop TCSPC hardware). To test the long-term stability of the measurement, data sets were taken with the SPADs both before and after acquiring data with the two-element SNSPD. Integrating the number of counts in a 2.4-ns window centered on the quantum dot intensity correlation peaks, we calculate $g^{(2)}(0)$ values (no background subtraction) using the SPADs of 0.10 ± 0.01 before and 0.15 ± 0.01 after the value of 0.12 ± 0.02 that was measured with the two-element SNSPD. Ideally, all three measurements would yield an identical value of $g^{(2)}(0)$; however, the two different results with SPADs indicate that $g^{(2)}(0)$ of the quantum dot source increased slightly over the course of the measurements. This increase was most likely due to small drifts in quantum dot temperature and alignment with respect to the pump beam. Such a drift can lead to small changes in the fraction of light incident on the detectors originating from the desired quantum dot emission line, relative to light from other emission lines from this or another quantum dot in the same micropillar. Even with this drift, the SNSPD result agrees with both results using SPADs, within the experimental uncertainties. Our inability to completely remove light from other emission lines is responsible for the measured nonzero values of $g^{(2)}(0)$.

Similarly, integrating the counts in a 1.6-ns window for the Ti:sapphire laser data results in $g^{(2)}(0)$ values of 1.003 ± 0.003 using the SPADs and 0.995 ± 0.004 using the two-element SNSPD. In all cases, the uncertainties account only for predicted statistical variations due to the finite number of measured correlation counts (see Ref. [7]) and not any systematic errors such as drift or detector and electronic dead times. Nevertheless, both of the laser measurements are in agreement with the expected $g^{(2)}(0) = 1$, roughly within the

expected statistical variation, and all the quantum dot measurements are consistent with a slow drift in the setup.

This agreement in measured $g^{(2)}(0)$ for the two techniques demonstrates that the two-element SNSPD does not exhibit measurable cross talk or introduce other measurement artifacts, which would alter the correlation counts at short time delays by increasing (or decreasing, depending on the mechanism) the probability of a nearly simultaneous switching event in the adjacent element. Furthermore, the agreement in $g^{(2)}(0)$, along with the lack of significant counts between peaks in the correlation histograms, indicates that the SNSPD dark-count rates are sufficiently low to permit measurements without background subtraction, as shown previously for single-element SNSPDs [7,9].

IV. CONCLUSION

In summary, the multielement SNSPD approach demonstrated here provides accurate intensity correlation measurements and offers several advantages over a free-space HBT interferometer. First, the multielement approach simplifies measurements over a wide range of wavelengths by requiring only a simple adjustment to the monochromator and the single necessary fiber. In the case of a standard HBT interferometer, it is important to ensure that both detectors are sampling the same spatial mode(s), which can be challenging with multimode sources, and it is also important to consider the range of wavelengths over which the beam splitter and optical coatings are suitable, in order to prevent artifacts from back-reflected photons in the interferometer. Furthermore, the broadband spectral response of SNSPDs and the lack of wavelength-dependent components make it easy to measure wavelengths throughout the visible and near infrared. Second, measurements of sources at telecommunication wavelengths could benefit from the low dark-count rate, short reset time, and continuous mode of detector operation. The smaller, low-inductance SNSPDs inherent to the multielement design enable precise timing resolution and fast reset times, which will be critical for measuring high-rate, nonclassical sources. Finally, measurements of higher-order correlation functions are possible using a detector with more elements. Four-element SNSPDs have been demonstrated [11] that will enable third- and fourth-order intensity correlation measurements without additional optical components, which will be described in future publications. Therefore, the multielement SNSPD approach demonstrated here enables intensity correlation measurements over a wide spectral and temporal range with high-speed, precise timing, minimal potential for measurement artifacts and no additional optical or active electrical components beyond those required for measuring PL lifetimes.

ACKNOWLEDGMENTS

The authors thank Dr. A. J. Kerman and Professor H. I. Smith for the use of their facilities and equipment and J. Daley for technical assistance. This work made use of MIT's shared scanning-electron-beam-lithography facility in the Research Laboratory of Electronics (SEBL at RLE). This work was sponsored by the United States Air Force under Air Force Contract No. FA8721-05-C-0002.

[1] R. Hanbury Brown and R. Q. Twiss, Nature (London) **177**, 27 (1956).
[2] H. J. Kimble, M. Dagenais, and L. Mandel, Phys. Rev. Lett. **39**, 691 (1977).
[3] R. Loudon, *The Quantum Theory of Light*, 3rd ed. (Oxford University Press, Oxford, 2000).
[4] F. T. Arecchi, E. Gatti, and A. Sona, Phys. Lett. **20**, 27 (1966).
[5] R. H. Hadfield, M. J. Stevens, S. S. Gruber, A. J. Miller, R. E. Schwall, R. P. Mirin, and S. W. Nam, Opt. Express **13**, 10846 (2005).
[6] M. J. Stevens, R. H. Hadfield, R. E. Schwall, S. W. Nam, and R. P. Mirin, IEEE J. Sel. Top. Quantum Electron. **12**, 1255 (2006).
[7] R. H. Hadfield, M. J. Stevens, R. P. Mirin, and S. W. Nam, J. Appl. Phys. **101**, 103104 (2007).
[8] A. Korneev, Y. Vachtomin, O. Minaeva, A. Divochiy, K. Smirnov, O. Okunev, G. Gol'tsman, C. Zinoni, N. Chauvin, L. Balet, R. Marsili, D. Bitauld, B. Alloing, L. Li, A. Fiore, L. Lunghi, A. Gerardino, M. Halder, C. Jorel, and H. Zbinden, IEEE J. Sel. Top. Quantum Electron. **13**, 944 (2007).
[9] C. Zinoni, B. Alloing, L. H. Li, F. Marsili, A. Fiore, L. Lunghi, A. Gerardino, Yu. B. Vakhtomin, K. V. Smirnov, and G. N. Gol'tsman, Appl. Phys. Lett. **91**, 031106 (2007).
[10] E. A. Dauler, B. S. Robinson, A. J. Kerman, J. K. W. Yang, K. M. Rosfjord, V. Anant, B. Voronov, G. Gol'tsman, and K. K. Berggren, IEEE Trans. Appl. Supercond. **17**, 279 (2007).
[11] E. A. Dauler, A. J. Kerman, B. S. Robinson, J. K. W. Yang, B. Voronov, G. Gol'tsman, S. A. Hamilton, and K. K. Berggren, e-print arXiv:physics/085.2397.
[12] A. J. Kerman, E. A. Dauler, W. E. Keicher, J. K. W. Yang, K. K. Berggren, G. Gol'tsman, and B. Voronov, Appl. Phys. Lett. **88**, 111116 (2006).
[13] M. J. Stevens, R. H. Hadfield, R. E. Schwall, S. W. Nam, R. P. Mirin, and J. A. Gupta, Appl. Phys. Lett. **89**, 031109 (2006).
[14] A. J. Kerman, E. A. Dauler, J. K. W. Yang, K. M. Rosfjord, K. K. Berggren, G. Gol'tsman, and B. Voronov, Appl. Phys. Lett. **90**, 101110 (2007).
[15] In this work, Perkin-Elmer SPCM-AQR SPADs and Picoquant PicoHarp 300 TCSPC hardware were used. These instruments are identified only to allow the measured IRF of the SPAD and the SNSPD, including the timing electronics, to be appropriately interpreted. Such identification does not imply that these instruments are necessarily the best available for this purpose.
[16] R. J. Molnar, E. A. Dauler, A. J. Kerman, J. K. W. Yang, S. A. Hamilton, and K. K. Berggren (unpublished).
[17] J. K. W. Yang, E. Dauler, A. Ferri, A. Pearlman, A. Verevkin, G. Gol'tsman, B. Voronov, R. Sobolewski, W. E. Keicher, and K. K. Berggren, IEEE Trans. Appl. Supercond. **15**, 626 (2005).